Mechanism of One-Electron Oxidation of NAD(P)H and Function of NADPH Bound to Catalase

Örn Almarsson, Ashoke Sinha, Enona Gopinath, and Thomas C. Bruice*

Contribution from the Department of Chemistry, University of California at Santa Barbara, Santa Barbara, California 93106

Received March 1, 1993

Abstract: Biologically important 1e⁻ oxidations of NAD(P)H are rare. Catalase compound II and $Fe(CN)_6^{3-}$ are both strong obligate 1e⁻ oxidants. Using *N*-methyl-1,10-dihydroacridan (MAH) and *N*-methyl-1,10-dideuterioacridan (MAD) as models for *N*-alkyl-1,4-dihydronicotinamide and *N*-alkyl-1,4-dideuterionicotinamide, the mechanism for oxidation has been shown to involve (i) 1e⁻ oxidation by $Fe(CN)_6^{3-}$ to yield the radical cation $MAH^{+\bullet}$; (ii) general-base-catalyzed proton abstraction from C10-H(D) of $MAH^{+\bullet}$ to provide the neutral radical MA•; and (iii) rapid 1e⁻ oxidation of MA• by $Fe(CN)_6^{3-}$ to provide the product *N*-methylacridinium cation (MA^+) (Scheme I). Rate constants for general-base catalysis of $MAH^{+\bullet} \rightarrow MA^\bullet$ by H_2O, formate, acetate and imidazole are associated with deuterium kinetic isotope effects (k_{MAH}/k_{MAD}) of ~7–10, 4.6, 5.4, and 5.6, respectively (Brønsted β value of 0.2). The magnitudes of the deuterium isotope effects and β when proton abstraction is rate limiting suggest the transition state for the proton transfer to involve tunneling and to be early. With the X-ray structure of bovine catalase (Rossmann et al, ref 5), the imidazole bases of His234 and His304 in the NADPH pocket are identified as possible general-base catalysts for $NADPH^{+\bullet} \rightarrow NADP^\bullet$ in the sequential $-1e^-, -1H^+, -1e^-$ oxidations of the NADPH moiety. Calculations of electron-tunneling pathways between NADPH (14DHN) and hypervalent iron protoporphyrin-IX (PP-IX) species were performed using PATHWAYS II (version 2.01). By use of X-ray and dynamics simulated structures, two major paths were identified: A, 14DHN–jump–Pro150–Thr149–jump–Asn147–jump–vinyl CH_2=CH– [PP-IX pyrrole ring C]–Fe, and B, 14DHN–jump–Pro150–Thr149–Hbond–Ser216–jump–CH_2=CH–[PP-IX pyrrole ring C]–Fe. Both paths involve short through-space jumps in addition to σ-tunnels. Pathway B also utilizes an Hbond between Thr149(C=O) and Ser216(O—H). In the X-ray structure paths A and B have nearly identical coupling efficiencies with the PP-IX ring and iron atom, but the dynamics simulated structure favors path B by 10-fold. The favoring of path B is the result of movement of the Asn147 sidechain away from PP-IX, along with shortening of the Thr149(C=O)–(HO)Ser216 interstrand hydrogen bond during MD. The calculated coupling elements associated with paths A and B were within 1 order of magnitude of the other, indicating that both pathways contribute substantially to the overall tunneling effect. Neither axial ligand on the iron (proximal Tyr357 or distal H_2O) takes part in electron transfers by the PATHWAYS II analysis. Conformational features (torsion angles X_n and X_{am} and puckering angles α_C and α_N, Chart I) of the 1,4-dihydronicotinamide (14DHN) nucleotide were analyzed from the dynamics structures. The average value of X_n of 96° dictates a *syn* conformation for the 14DHN nucleotide, with the *pro-S* hydrogen (H_S) on C4 of 14DHN pointed in the direction of iron protoporphyrin-IX (PP-IX). X_{am} values observed during MD (between 126 and 174°) indicate that the C=O of the $CONH_2$ remains *trans* to C2 (Chart III) and on the B-face adjacent to H_S throughout MD. The puckering angles α_C and α_N (Chart I) have average values of 7 and 13°, respectively, where N1 and C4 of 14DHN are displaced out of the plane of the ring to a quasi-boat form. Anisotropy of the quasi-boat conformation points the "bow and stern" of the quasi-boat (C4 and N1) toward the PP-IX with H_S pseudo-axial. It is suggested that NADPH in catalase acts not only as a rescuer of inactive catalase (in the compound II state) but also as a fuse for active catalase (in the compound I state) in the presence of very low concentrations of H_2O_2.

Introduction

Catalase efficiently catalyzes the disproportionation of hydrogen peroxide to water and dioxygen (eq 1a,b).[1] The proto-

$$\text{catalase} + H_2O_2 \rightarrow \text{compound I} + H_2O \quad (1a)$$

$$\text{compound I} + H_2O_2 \rightarrow \text{catalase} + H_2O + O_2 \quad (1b)$$

porphyrin-IX iron(III) (PP-IX) at the active site of resting catalase reacts with hydrogen peroxide to give a hypervalent iron porphyrin species (Compound I) and a molecule of water through what is overall a heterolytic scission of the peroxide O–O bond (eq 1a).[2] Compound I[1] is 2 oxidation equivalents above the resting protoporphyrin-IX iron(III) state and has been shown by a variety of spectroscopic methods to be an iron(IV) oxo porphyrin π-cation radical.[3] This species is the active oxidant, which reacts with another molecule of H_2O_2 to give dioxygen and water (eq 1b) or oxidizes another small substrate molecule. Compound I reacts, for example, with ethanol to give acetaldehyde (eq 2).[1] A second

$$\begin{array}{ccc} \text{catalase–(porph}^{\bullet+}\text{)Fe}^{IV}\text{O} & & \text{catalase–(porph)Fe}^{III} \\ + & \rightarrow & + \\ CH_3CH_2OH & & CH_3CHO \end{array} \quad (2)$$

hypervalent iron porphyrin species, compound II, can form *via* one- electron reduction of compound I and it is an iron(IV) oxo ligated porphyrin (eq 3). Compound II does not take part in the catalytic cycle of the reaction of catalase with hydrogen peroxide, and its accumulation leads to inactivation of the enzyme.

(1) Schonbaum, G. R.; Chance, B. In *The Enzymes*, 2nd ed.; Boyer, P. D., Ed.; Academic Press: New York, 1976; Vol. 13, pp 363–408.

(2) For recent reviews of reactions of hydroperoxides with iron(III) porphyrins and other metalloporphyrins, see: (a) Bruice, T. C. *Acc. Chem. Res.* **1991**, *24*, 243. (b) Bruice, T. C. In *Mechanistic Principles of Enzymatic Activity*; Liebman, J. F., Greenberg, A., Eds.; VCH Publishers Inc.: Deerfield Beach, FL, 1988; Chapter 6, pp 227–277. (c) Bruice, T. C. *Aldrichimica Acta* **1988**, *21*, 87.

(3) (a) Dolphin, D.; Forman, A.; Borg, D. C.; Fajer, J.; Felton, R. H. *Proc. Natl. Acad. Sci. U.S.A.* **1971**, *68*, 614. (b) Moss, T. H.; Ehrenberg, A.; Beardon, A. J. *Biochemistry* **1969**, *8*, 4159. (c) Schulz, C. E.; Devaney, P. W.; Winkler, H.; Debrunner, P. G.; Doan, N.; Chiang, R.; Rutter, R.; Hager, L. P. *FEBS Lett.* **1979**, *103*, 102. (d) Roberts, J. E.; Hoffman, B. M.; Rutter, R.; Hager, L. P. *J. Biol. Chem.* **1981**, *256*, 2118.

0002-7863/93/1515-7093$04.00/0

$$\text{catalase–(porph}^{+\bullet})\text{Fe}^{IV}\text{O} + 1e^- \rightarrow \text{catalase–(porph)Fe}^{IV}\text{O} \quad (3)$$
(compound I) (compound II)

In 1984, Kirkman[4] and co-workers discovered the presence of tightly bound 1,4-dihydronicotinamide adenine dinucleotide 2-phosphate (NADPH) in bovine catalase. NADPH was found to be preferentially bound over $NADP^+$ by several orders of magnitude. Reevaluation of the high-resolution X-ray structure for bovine catalase unequivocally established the presence of NADPH in each subunit of the tetrameric protein.[5] Human erythrocyte, canine,[4] and *Pseudomonas mirabilis*[6] catalases have subsequently been shown to bind NADPH, but the dinucleotide is known to be absent in catalase from *Pseudomonas vitale*.[7]

The present study is concerned with the mechanism and role of the NADPH cofactor in catalase, which has been investigated by (i) using $Fe(CN)_6^{3-}$ as a surrogate of compound II in kinetic studies[8] and (ii) computational methods with the X-ray structure of bovine catalase by Rossmann.[5] Electronic coupling factors for the weakly coupled donor–acceptor pair NADPH–[PP-IX]Fe were calculated using the recently developed PATHWAYS II program of J. J. Regan,[9] and probable electron-tunneling pathways were identified using this approach. Initial structures for pathway calculations were generated by $CHARM_m$[10] molecular dynamics simulation using the catalase X-ray structure.[5] Boat conformations of the 1,4-dihydronicotinamide ring are of interest in NAD(P)H oxidations.[11] Ab initio calculations with *N*-methyl-1,4-dihydronicotinamide {MNic and MNic(bent)} at the 3-21G* level in the Gaussian 90 program[12] were performed to calculate relative stabilities of planar and quasi-boat conformations of the neutral systems and the radical cations $MNic^{+\bullet}$ and $MNic(bent)^{+\bullet}$ formed by one-electron oxidation of MNic and MNic(bent), respectively. Further, possible general bases in the NADPH binding site, capable of catalyzing the electron-transfer reactions, are identified from the molecular dynamics simulation.

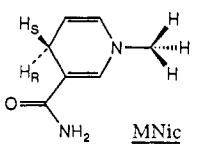

MNic

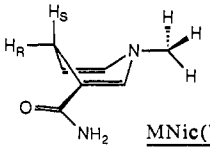

MNic(bent)

Experimental Section

Solution Kinetics. Reactions of *N*-methyl-1,10-dihydroacridan (MAH) (and *N*-methyl-1,10-dideuterioacridan (MAD)) with $K_3Fe(CN)_6$ were run in 20:80 acetonitrile–water mixtures at 30 °C, as described previously by Powell et al.,[13] using formate, acetate, and imidazole buffers under pseudo-first-order conditions ($[Fe(CN)_6^{3-}] \gg [MAH] = 4.7 \times 10^{-6}$ M $\ll [Fe(CN)_6^{4-}]$ with $[K^+] = 0.75$ M). The increase in visible absorbance at 359 nm (product *N*-methylacridinium cation (MA^+)) was followed.

Computational Methods. $CHARM_m$ version 21.3 molecular dynamics were run on the Silicon Graphics 4D/340GTX workstation, and structural visualization and manipulation were performed in Quanta (Polygen-MSI, Waltham, MA). The coordinate file *pdb7cat.ent*[5] was extracted from the Brookhaven Database.[14] Only polar hydrogens were added to the enzyme structure; extended atoms were used for all carbon chains. Certain simplifications of the structure were made to decrease the computational task: The N-terminus was truncated (from residue 1 to 66) such that the new N-terminal residue is Arg67. The hinge region[5] which connects two subunits to make half of the native tetrameric protein was removed to provide two units of protein: Deletion of residues 380–416 resulted in the former Arg379 becoming a carboxy terminus and the former Ala417 being an N-terminus. N-termini were furnished with protons to provide ammonium ions, while C-termini were left as $-CO_2^-$. These provisions significantly simplified the computational effort and are justified in view of the fact that a single subunit is being considered (i.e., no hinge peptide is needed). The $CHARM_m$ topology file AMINO.RTF was used for the remaining enzyme residues. All histidines were treated as $CHARM_m$ residue HIS, in the preferred δ-protonated tautomer form. Water molecules were treated as TIP3P residues.[15] The NADPH cofactor unit was modified to include all hydrogens. A $CHARM_m$ atom type CUA1 was used for carbons 2, 3, 5, and 6 of the 1,4-dihydronicotinamide of NADH, and NP was used for the pyridine nitrogen. The parameter file PARM. PRM was modified to include the following angle parameters: (a) (pyrophosphate) O–P–O = 112.0°,[16a] force constant 100.0 kcal/(mol Å) and (b) (14DHN) CUA1–NP–CUA1 = 117.2°, force constant 120.0 kcal/(mol Å).[16b] Partial charges for NADPH were obtained by AM1 calculation of the structure as it appears in the catalase crystal structure (1SCF calculation), after $CHARM_m$ minimization of added hydrogens only. Protoporphyrin-IX was also furnished with all hydrogens; a residue name HEM from the topology file PORPHYRINH.RTF (Polygen-MSI) was used as a basis for the iron porphyrin. HEM describes Fe(II) porphyrin; hence, HEM was modified to have a +3 charge on the iron, and the total charge on the residue was changed to −1.0. Prior to minimization, it proved necessary to apply light distance constraints on the position of the iron atom of protoporphyrin-IX: Each of the four N–Fe bonds was set to be 2.00 Å with an allowable ±0.05-Å fluctuation, a scale of 30 was applied, and a temperature of 300 K was stipulated. The complete assembly was minimized prior to dynamics studies: 100 steps of steepest descents algorithm minimization with a force criterion of 0.001 kcal/10 steps were followed by adopted basis Newton–Raphson algorithm for 2000 steps (tolerance 1×10^{-9} kcal/10 steps). Hydrogen bonds and nonbonding interactions were cut off at 5.0 and 14.0 Å, respectively, and were updated every 25 steps. Dynamics to 80 ps using a timestep of 0.001 ps (1000 steps/ps) were run using Verlet integration. The following protocol was used: a heating phase of 3 ps to a final temperature of 300 K, followed by equilibration of 57 ps, and finally 20 ps of observation. Coordinates were printed every 0.05 ps, rendering 400 structures from the 20 ps of collection phase.

Gaussian 90 3-21G* calculations[12] were carried out on a Vax station 3100. The input structure and initial parameters were obtained from AM1 calculations of MNic and $MNic^{+\bullet}$ with full optimization of each structure to planar conformations. MNic(bent) and $MNic(bent)^{+\bullet}$ were constructed from MNic and $MNic^{+\bullet}$ on Silicon Graphics 3D/340GTX in Quanta (Polygen-MSI) with special attention to keeping bond lengths unchanged compared with the planar structures. Full optimization of all parameters at the 3-21G* level was allowed for MNic and $MNic^{+\bullet}$, whereas positions of ring atoms in MNic(bent) and $MNic(bent)^{+\bullet}$ were fixed. Heats of formation were not corrected for ZPE, but differences between planar and boat forms were calculated and multiplied by 627.51 kcal/hartree.

(4) Kirkman, H. N.; Gaetani, G. F. *Proc. Natl. Acad. Sci. U.S.A.* **1984**, *81*, 4343.

(5) (a) Murthy, M. R. N.; Reid, T. J., III; Sicignan, A.; Tanaka, N.; Rossmann, M. G. *J. Mol. Biol.* **1981**, *152*, 465. (b) Fita, I.; Rossmann, M. G. *Proc. Natl. Acad. Sci. U.S.A.* **1985**, *82*, 1604.

(6) Jouve, H. M.; Beaumont, F.; Leger, I.; Foray, J.; Pelmont, J. *Biochem. Cell Biol.* **1989**, *67*, 271.

(7) Melik-Adamyan, W. R.; Barynin, V. V.; Vagin, A. A.; Borisov, V. V.; Vainshtein, B. K.; Fita, I.; Murthy, M. R. N; Rossmann, M. G. *J. Mol. Biol.* **1986**, *188*, 63.

(8) Some of these results have appeared in a preliminary communication: Sinha, A.; Bruice, T. C. *J. Am Chem. Soc.* **1984**, *106*, 7291.

(9) Regan, J. J. *PATHWAYS II software*, version 2.01; University of California—San Diego: San Diego, CA, 1993.

(10) Brooks, B. R.; Bruccoleri, R. E.; Olafson, B. D.; States, D. J.; Swaminathan, S.; Karplus, M. *J. Comput. Chem.* **1983**, *4*, 187.

(11) (a) Almarsson, Ö.; Bruice, T. C. *J. Am. Chem. Soc.* **1992**, *114*, 8702 and references therein. (b) Almarsson, Ö.; Bruice, T. C. *J. Am. Chem. Soc.* **1993**, *115*, 2125.

(12) Frisch, M. J.; Head-Gordon, M.; Trucks, G. W.; Foresman, J. B.; Schlegel, H. B.; Raghavachari, K.; Robb, M.; Binkley, J. S.; Gonzalez, C.; Defrees, D. J.; Fox, D. J.; Whiteside, R. A.; Seeger, R.; Melius, C. F.; Baker, J.; Martin, R. L.; Kahn, L. R.; Stewart, J. J. P.; Topiol, S.; Pople, J. A. *Gaussian 90 program*, revision F; Gaussian, Inc.: Pittsburgh, PA, 1990.

(13) Powell, M. F.; Wu, J. C.; Bruice, T. C. *J. Am. Chem. Soc.* **1984**, *106*, 3850.

(14) Brookhaven database, July 1991 release. (a) Brenstein, F. C.; Koetzle, T. F.; Williams, G. J. B.; Meyer, E. F., Jr.; Brice, M. D.; Rodgers, J. R.; Kennard, O.; Shimanouchi, T.; Tasumi, M. *J. Mol. Biol.* **1977**, *112*, 535. (b) Abola, E.; Bernstein, F. C.; Bryant, S. H.; Koetzle, T. F.; Weng, J. In *Crystallographic Databases—Information Content, Software Systems, Scientific Applications*; Allen, F. H., Bergerhoff, G., Sievers, R., Eds.; Data Commission of the International Union of Crystallography: Bonn, Cambridge, Chester, 1987; pp 107–132.

(15) Jorgensen, W. L.; Chandrasekar, J.; Madura, J. D. *J. Phys. Chem.* **1983**, *79*, 926.

(16) (a) An average value from the two O–P–O angles in NADPH in the Brookhaven datafile *pdb7cat.ent* (ref 5). (b) See: Glasfeld, A.; Zbinden, P.; Dobler, M.; Benner, S. A.; Dunitz, J. D. *J. Am. Chem. Soc.* **1988**, *110*, 5152.

PATHWAYS II (version 2.01)[9] was implemented on Silicon Graphics 4D/340GTX, and Protein Data Bank format (pdb) files were used as input structures. Visualization of structures and pathways (from .usr files generated by the PATHWAYS program) was performed in InsightII Viewer (version 2.1.2., Biosym Technologies, San Diego, CA). Selected structures from the $CHARM_m$ molecular dynamics simulation, as well as the X-ray structure of catalase, were considered. A potential input file for NADPH was constructed and is available as supplementary material. The first part of the program, b2n, was run to generate covalent, hydrogen bond, and through-space connectivities with the following criteria: maximum distance through space of 5.0 Å, jump criterion enabled, fall-off percentage 30%, hydrogen and lone-pair addition enabled. Hydrogens and lone pairs were added to the entire structure as dictated by parameters from the potential input file. The second part of the program, n2p, was used to evaluate the pathways dominating the tunneling matrix by calculating coupling elements ϵ. Any coupling smaller than $\epsilon = 10^{-8}$ was considered negligible. The target orbitals selected in separate calculations were (a) HEM:CAC-HQ22, to reflect efficiency of electron transfer to the C ring vinyl $H_2C{=}CH$- closest to NADPH as a means of reducing compound I porphyrin π-cation radical, and (b) HEM:NC-HL3, to reflect electron transfer to the iron center to effect metal-centered reduction of Fe(IV)-species like compound II. In either case, the starting orbital was defined as C4-H_S (*pro-S* hydrogen on C4 of 1,4-dihydronicotinamide) on NADPH. A β-value of 1.7 was used as a standard driving force in the general distance-dependent coupling relation (eq 4):[17]

$$\epsilon^{TS/HB} = \text{prefactor} \exp[-\beta(r - r_{eq})] \quad (4)$$

The square of ϵ is proportional to the rate constant for electron transfer.[17d] In every calculation, a fixed decay factor was used for covalent bond interactions ($\epsilon^{COV} = 0.6$, with $\beta = 0$), while hydrogen bonds ($r_{eq} = 2.8$, prefactor = 0.6) and through-space links ($r_{eq} = 1.4$, prefactor = 0.6) cause an exponential decay of coupling according to eq 4.

Results

Kinetics of oxidation and nature of general-base catalysis in the reactions of *N*-methyl-1,10-dihydroacridan (MAH) and

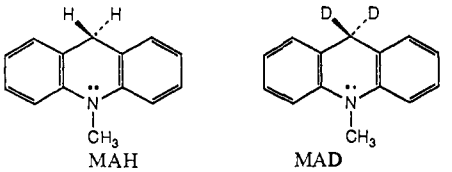

N-methyl-1,10-dideuterioacridan (MAD) with the obligate one-electron oxidant $Fe(CN)_6^{3-}$ (eq 5) were studied under an oxygen-

$$MAH + 2Fe(CN)_6^{3-} \rightarrow MA^+ + 2Fe(CN)_6^{4-} + H^+ \quad (5)$$

free nitrogen atmosphere in 20:80 acetonitrile–water (v/v) at 30 ± 0.1 °C. Pseudo-first-order conditions of $[Fe(CN)_6^{3-}] \gg [MAH] = 4.7 \times 10^{-6}$ M $\ll [Fe(CN)_6^{4-}]$ with $[K^+] = 0.75$ M were employed. The time courses of the reactions were followed by monitoring the increase in absorbance at 359 nm due to the product *N*-methylacridinium cation (MA^+). The appearance of MA^+ obeyed the first-order rate law to completion of reaction in all cases. The dependence of observed pseudo-first-order rate constants for the oxidation of MAH (k^H_{obsd}) and MAD (k^D_{obsd}) upon buffer concentration was investigated over a range of constant pH values and, unless stated otherwise, at fixed concentrations of $Fe(CN)_6^{3-}$ (8.0×10^{-4} M) and $Fe(CN)_6^{4-}$ (1.5×10^{-4} M). The values of k^H_{obsd} and k^D_{obsd} were linearly dependent on buffer concentration, at all pH values and concentrations of buffers investigated. The buffer systems employed were imidazole/imidazolium cation (pH 6.3–7.7), acetate/acetic acid (pH 4.5–5.8), and formate/formic acid (pH 3.3–4.6). For each buffer,

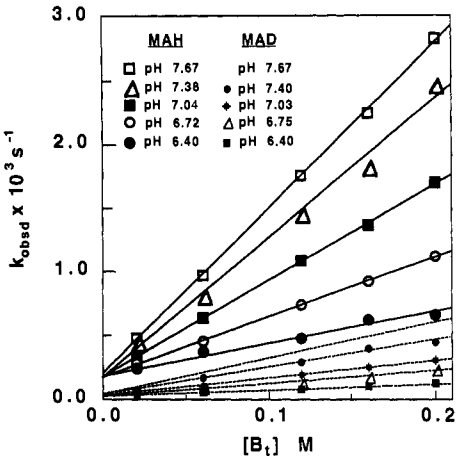

Figure 1. Plots of k^H_{obsd} (solid lines) and k^D_{obsd} (dashed lines) vs the total concentration of formate buffer ([B_t]) used at μ = 0.75 and 30 °C.

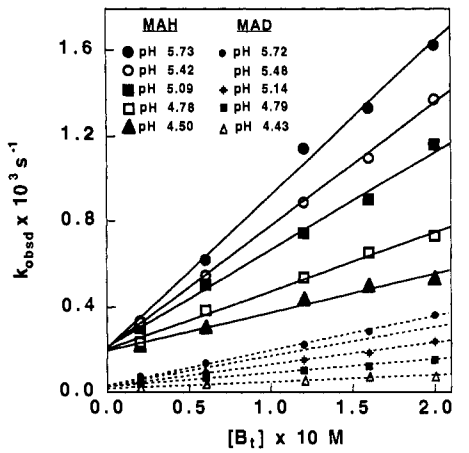

Figure 2. Plots of k^H_{obsd} (solid lines) and k^D_{obsd} (dashed lines) vs the total concentration of acetate buffer ([B_t]) used at μ = 0.75 and 30 °C.

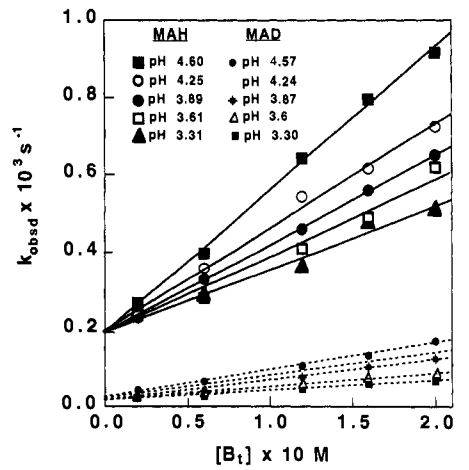

Figure 3. Plots of k^H_{obsd} (solid lines) and k^D_{obsd} (dashed lines) vs the total concentration of imidazole buffer ([B_t]) used at μ = 0.75 and 30 °C.

reactions were carried out at five pH values, and at each pH reactions were studied at five total buffer, [B_t] (=[BH] + [B]), concentrations which ranged over a 10-fold change (0.02–0.2 M). The slopes of the linear plots (Figures 1–3) of pseudo-first-order rate constants (k^H_{obsd} and k^D_{obsd}) for MA^+ appearance vs [B_t] provide pH-dependent apparent second-order rate constants ($k^H_{B_t}$ and $k^D_{B_t}$) for the buffer-catalyzed oxidation of MAH and MAD. The values at the intercepts of the plots were, within experimental error, pH independent and gave rate constants for H_2O-catalyzed oxidation of MAH (k^H_{ly}) or MAD (k^D_{ly}) (eq 6a,b).

(17) (a) Beratan, D. N.; Onuchic, J. N.; Winkler, J. R.; Gray, H. B. *Science* **1992**, *258*, 1740. (b) Onuchic, J. N.; Beratan, D. N.; Winkler, J. R.; Gray, H. B. *Annu. Rev. Biophys. Biomol. Struct.* **1992**, *21*, 349. (c) Beratan, D. N.; Betts, J. N.; Onuchic, J. N. *Science* **1991**, *252*, 1285. (d) Sutin, N.; Marcus, R. N. *Biophys. Biochim. Acta* **1985**, *811*, 265.

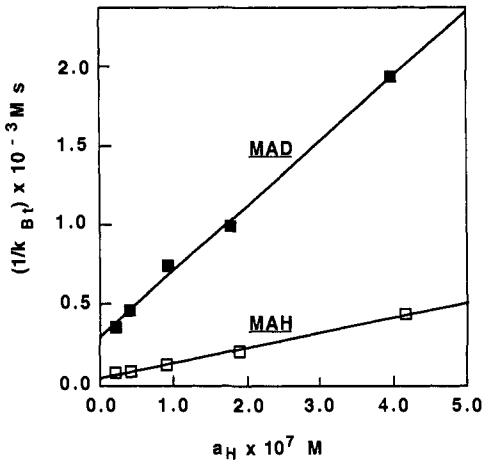

Figure 4. Plots of $1/k^{H}_{Bt}$ and $1/k^{D}_{Bt}$ vs a_H in imidazole buffers, at μ = 0.75 and 30 °C. The plots are linear with a positive slope, implicating the buffer base species as the catalytic entity. The intercepts on the y-axis provide the inverse of the second-order rate constant for catalysis by general base ($1/k_B$).

Table I. Second-Order Rate Constants k_B^H and k_B^D for the General-Base-Catalyzed Oxidation of MAH and MAD by $[Fe(CN)_6]^{3-}$

buffer system	k_B^H (M^{-1} s^{-1})	k_B^D (M^{-1} s^{-1})	k_B^H/k_B^D
HCO_2^-/HCO_2H	3.3×10^{-3}	7.2×10^{-4}	4.6
$CH_3CO_2^-/CH_3CO_2H$	8.6×10^{-3}	1.6×10^{-3}	5.4
ImH/ImH_2^+	1.9×10^{-2}	3.4×10^{-3}	5.6

$$k^{H}_{obsd} = k^{H}_{ly} + k^{H}_{B_t}[B_t] \quad (6a)$$

$$k^{D}_{obsd} = k^{D}_{ly} + k^{D}_{B_t}[B_t] \quad (6b)$$

From the determined values of k^{H}_{ly} and k^{D}_{ly} there were calculated deuterium isotope effects (k^{H}_{ly}/k^{D}_{ly}) of 9.9, 7.4, and 6.5 for reactions carried out in formate, acetate, and imidazole buffers, respectively. The dependencies of the apparent second-order rate constants, $k^{H}_{B_t}$ and $k^{D}_{B_t}$, on a_H are described by eq 7a,b, where K_a is the acid dissociation constant of the conjugate

$$k^{H}_{B_t} = \frac{k_B^H K_a}{(K_a + a_H)} \quad (7a)$$

$$k^{D}_{B_t} = \frac{k_B^D K_a}{(K_a + a_H)} \quad (7b)$$

acid of the buffer base and k_B^H and k_B^D are second-order rate constants for buffer base species. From the inverse expression of eq 7a,b, plots of $1/k^{H}_{B_t}$ vs a_H and $1/k^{DBt}$ vs a_H are linear, and intersect the y-axis at $1/k_B^H$ and $1/k_B^D$, respectively. Figure 4 shows such linear plots for the imidazole-catalyzed reactions of MAH and MAD. From the values of k_B^H and k_B^D in Table I, the deuterium isotope effects on the second-order rate constants for buffer base catalysis (k_B^H/k_B^D) are 4.6, 5.4, and 5.6 for formate, acetate, and imidazole, respectively.

Buffer base catalysis of the oxidation of MAH (and MAD) is accommodated by the sequence of reactions shown in Scheme I. With the steady-state assumption in radical cation, $MAH^{+\bullet}$, Scheme I provides eq 8. With the further assumption that

$$k_{obsd} = \frac{k_1[Fe(CN)_6^{3-}](k_0 + k_2[B])}{k_{-1}[Fe(CN)_6^{4-}] + (k_0 + k_2[B])} \quad (8)$$

$k_{-1}[Fe(CN)_6^{4-}] \gg (k_0 + k_2[B])$, eq 8 is reduced to eq 9a, which predicts the experimentally observed linear dependence of k_{obsd}

Scheme I

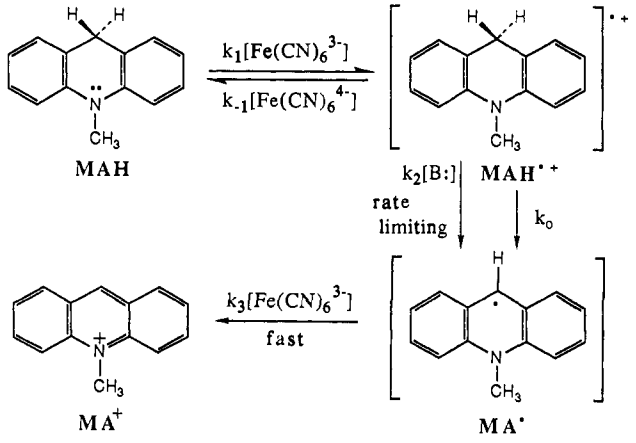

$$k_{obsd} = \frac{k_1[Fe(CN)_6^{3-}]}{k_{-1}(Fe(CN)_6^{4-}]}(k_0 + k_2[B]) \quad (9a)$$

$$k_{obsd} = \frac{k_1[Fe(CN)_6^{3-}]}{k_{-1}[Fe(CN)_6^{4-}]}\left\{k_0 + \frac{k_2K_a[B_t]}{(K_a + a_H)}\right\} \quad (9b)$$

on [B]. Comparison of eq 9 to eqs 6 and 7 provides the equalities of eq 10a–c. Inverting eq 8 provides eq 11, which predicts a

$$k_{ly} = \left(\frac{k_1[Fe(CN)_6^{3-}]}{k_{-1}[Fe(CN)_6^{4-}]}\right)k_0 \quad (10a)$$

$$k_B = \left(\frac{k_1[Fe(CN)_6^{3-}]}{k_{-1}[Fe(CN)_6^{4-}]}\right)k_2 \quad (10b)$$

$$k_{B_t} = \left(\frac{k_1[Fe(CN)_6^{3-}]}{k_{-1}[Fe(CN)_6^{4-}]}\right)\frac{k_2Ka}{(K_a + a_H)} \quad (10c)$$

$$1/k_{obsd} = \frac{k_{-1}[Fe(CN)_6^{4-}]}{k_1[Fe(CN)_6^{3-}](k_0 + k_2[B])} + \frac{1}{k_1[Fe(CN)_6^{3-}]} \quad (11)$$

linear dependence of $1/k_{obsd}$ on $[Fe(CN)_6^{4-}]$, if pH, $[B_t]$, and $[Fe(CN)_6^{3-}]$ are kept constant. The value of k_1 may be determined from the intercept of a plot of $1/k_{obsd}$ vs $[Fe(CN)_6^{4-}]$. A set of experiments was carried out where $[Fe(CN)_6^{4-}]$ was varied from 6×10^{-5} M to 6×10^{-4} M, at pH 7.05 with a total imidazole buffer concentration ($[Im_t]$) = 2×10^{-2} M and $[Fe(CN)_6^{3-}]$ = 8×10^{-4} M. The linear plot of $1/k_{obsd}$ vs $[Fe(CN)_6^{4-}]$ is shown in Figure 5. A value $k_1 = 3.2$ M^{-1} s^{-1} was determined from the intercept of Figure 5. From the experimentally determined values of k_1 and k_2^H (Table I) and the known value of the "redox buffer ratio" $[Fe(CN)_6^{3-}]/[Fe(CN)_6^{4-}]$ (=5.4), values of the partition ratios k_2/k_{-1} were calculated to be 1.9×10^{-4}, 5.0×10^{-4}, and 1.1×10^{-3} from the experiments in formate, acetate, and imidazole buffers, respectively. Since k_{-1} is buffer independent, Brønsted slopes for general-base catalysis of the deprotonation of $MAH^{+\bullet}$ can be obtained from plots of $\log(k_2/k_{-1})$ vs the pK_a values of the buffer acids. From the data for catalysis by H_2O, HCO_2^-, $CH_3CO_2^-$, and ImH, the Brønsted β value equals ~0.2.

Molecular dynamics simulations of catalase including bound NADPH and iron(III) protoporphyrin-IX were carried out using $CHARM_m$[10] and the structural coordinates of the X-ray structure of bovine liver catalase.[5] No attempt was made to derive parameters to accommodate the oxidation states of compounds I and II. It is simply assumed that the tertiary structure of the

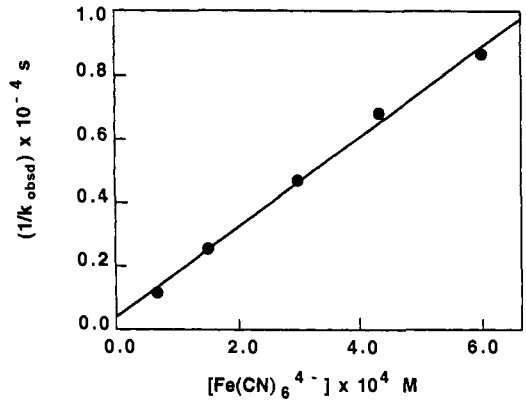

Figure 5. Plot of the reciprocal of the pseudo-first-order rate constant ($1/k_{obsd}$) vs $[Fe(CN)_6]^{4-}$ for the oxidation of *N*-methyl-1,10-dihydroacridan (MAH) by $Fe(CN)_6^{3-}$ (8×10^{-4} M) at pH 7.05 with total imidazole buffer ($[Im]_t$) = 2×10^{-2} M.

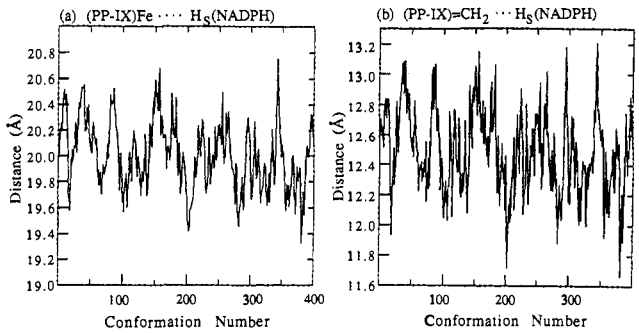

Figure 6. Calculated interatomic distances between NADPH and porphyrin in catalase from $CHARM_m$ molecular dynamics 20-ps sampling phase: (a) C4-H_S(nicotinamide) to Fe(protoporphyrin-IX); (b) C4-H_S(nicotinamide) to CH_2=(vinyl on ring c of protoporphyrin-IX).

Chart I

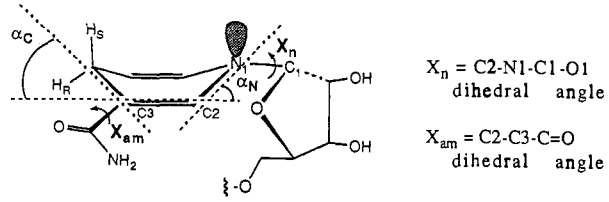

protein is not significantly altered on change in the oxidation state of the iron protoporphyrin-IX. Analysis of the 1,4-dihydronicotinamide conformation with time was carried out in order to understand the relationship between conformation (Chart I) and the facility for electron transfer. Dynamic trajectories for the resting state of the enzyme at 300 K to 80 ps were calculated with polar hydrogens on the enzyme structure; an extended atom force field was used for other hydrogens. All required parameters for NADPH and iron(III) protoporphyrin-IX, with +3 charge, were furnished with all hydrogen atoms in $CHARM_m$ (see Experimental Section). Basic amino acid side chain substituents were looked for in the vicinity of the C4 position of the nicotinamide ring in order to delineate possible general-base catalysts.

A. Spatial Relationship between NADPH and Protoporphyrin-IX. In Figure 6a and b are plotted the conformation numbers against the interatomic distances between (a) C4-H_S(nicotinamide) and the iron of iron(III) protoporphyrin-IX and (b) C4-H_S(nicotinamide) and H_2C=(vinyl on ring C of protoporphyrin-IX). The separation between the 1,4-dihydronicotinamide ring and the porphyrin is observed to be around 12.5 Å on average with a minimum value of 11.6 Å observed in MD (Figure 6b). Assuming that NADPH is placed in catalase to destroy unwanted or unusually long-lived hypervalent iron porphyrins, any hydride or electron transfer from NADPH to an oxidizing species must

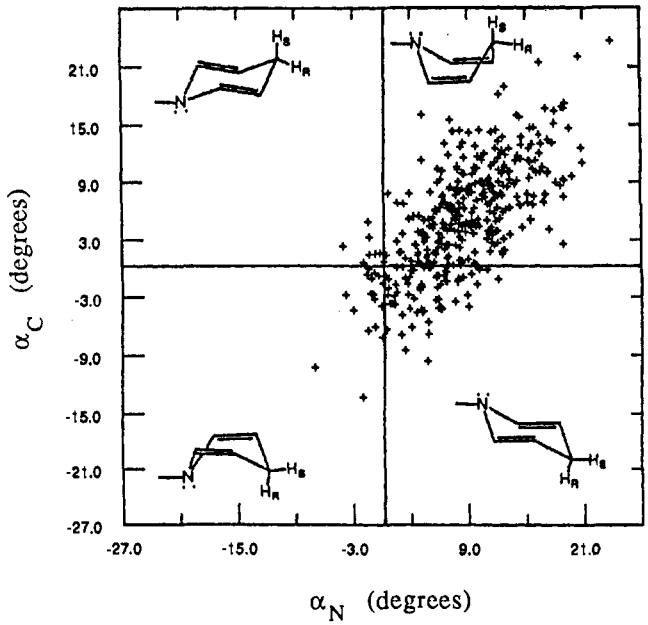

Figure 7. Plot of puckering angles α_C vs α_N from $CHARM_m$ molecular dynamics of catalase, 20-ps sampling phase (see Chart I and Experimental Section for definition of α_C and α_N). Positive α_C and α_N values (upper right hand corner) indicate the propensity for the quasi-boat conformation for the 1,4-dihydronicotinamide ring of NADPH, with the "bow and stern" of the boat pointing toward the iron porphyrin.

Chart II

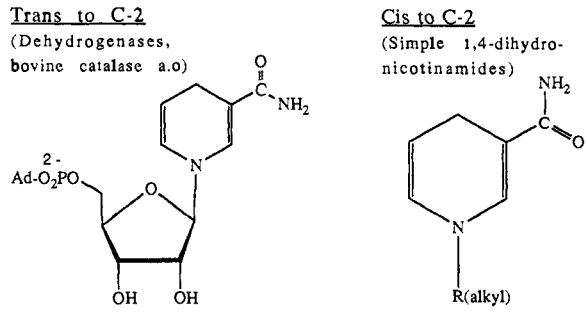

take place over this distance. In view of the small distance variations (±1 Å) in the MD structures when compared with the X-ray structure, hydride transfer can be regarded as impossible. The short deBroglie wavelength of the proton compared with that of the electron precludes tunneling over distances as great as 11 Å. A means by which electron tunneling can take place between cofactors was sought. A feature of interest is the peptide loop, which separates NADPH and the porphyrin (Chart III). The sequence Pro150-Thr149-Asn148-Asn147 passes between the two cofactors and provides, a priori, one possible pathway for electron transfer from NADPH to hypervalent iron protoporphyrin species.

B. NADPH Conformational Parameters. The degree of puckering of the 1,4-dihydropyridine ring toward a quasi-boat form is defined by α_C and α_N (Chart I). In a quasi-boat conformation one of the two prochiral hydrogens becomes pseudo-axial, while the other occupies a pseudo-equatorial position. The catalase structures generated from molecular dynamics show a persistent anisotropic puckering of the 1,4-dihydronicotinamide ring to a quasi-boat form, placing H_S in the pseudo-axial position. Figure 7 shows a plot of α_C vs α_N, generated by monitoring two improper dihedral angles on the 1,4-dihydropyridine ring of NADPH (C4–C5–C6–C2 for α_C and N1–C2–C3–C5 for α_N) through the sampling phase of MD. Average values for α_C and α_N are found to be 7° and 13°, respectively. In contrast to the observations with dehydrogenases,[11] the anisotropy of the [planar → boat] conformational change is caused by the steric require-

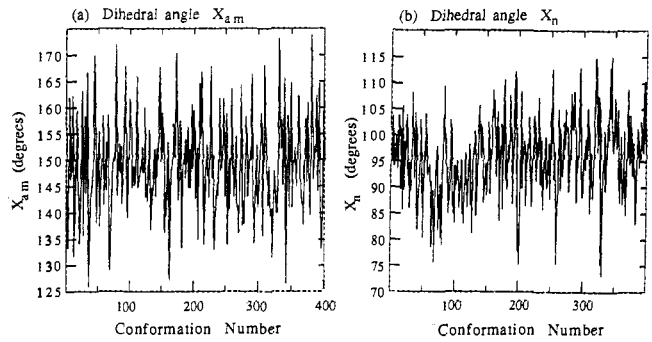

Figure 8. Variation of torsion angles of NADPH in catalase during $CHARM_m$ molecular dynamics, 20-ps sampling phase: (a) X_{am}; (b) X_n (see Chart I for definition of X_{am} and X_n).

Chart III

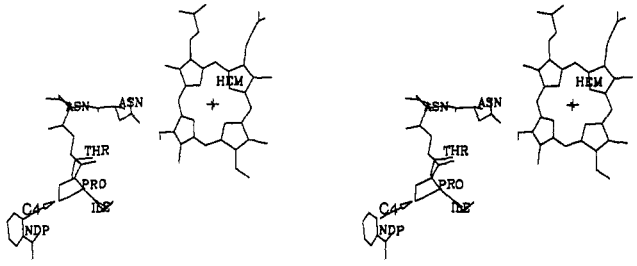

Scheme II

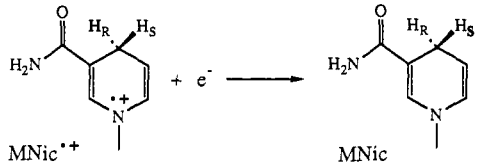

ments of the adenosine ribose ring of NADPH rather than the steric requirements of bulky aliphatic side chains of the protein structure. The average value of torsion angle X_{am} in the MD simulation (Chart I) is 149°. This so-called *trans* conformation (Chart II) has been determined to be a local minimum on the AM1 potential energy surface for the 1,4-dihydronicotinamides.[18] Figure 8a shows the evolution of X_{am} as a function of MD trajectory. Interestingly, the amide resides with the C=O bond on the B-side of the dihydronicotinamide ring (126° < X_{am} < 174°), adjacent to the *pro-S* hydrogen and is apparently not permitted to swing to the other side of the ring as in lactate dehydrogenase.[11b]

Ab initio calculations in the 3-21G* basis set using the Gaussian 90 program were carried out to determine the influence of conformation of the 1,4-dihydronicotinamide ring (flat and quasi-boat) on the potential for the 1e$^-$ reduction of NADPH (Scheme II). Table II summarizes the results of the calculations, which were carried out in the restricted Hartree–Fock (RHF) method for neutral species and unrestricted HF (UHF) method for both neutral species and radical cations. Cummins and Gready have studied the ground-state MNic in detail, and our results are in good agreement with their previous calculations.[18] The optimized geometry for the radical cation MNic$^{+\cdot}$ is available as supplementary material. The heats of formation in Table II do not appear to depend on the use of HF or UHF for the neutral species. The magnitudes of the oxidation potentials (ΔH_f) of Table II reflect gas-phase values, and only $\Delta\Delta H_f$ values serve our useful purpose. When comparing differences in heats of formation ($\Delta\Delta H_f$) of quasi-boat and flat nicotinamide rings, the results indicate that puckering of the radical cation to a quasi-boat (4.5 kcal/mol at 3-21G* geometry, UHF doublet spin state) is more energetically costly than like puckering of the neutral ground

(18) Cummins, P. L.; Gready, J. E. *THEOCHEM* **1989**, *183*, 161.

Table II. Ab Initio 3-21G* Calculated Heats of Formation for MNic and MNic(boat) Neutral Ground State and Radical Cations[a]

model	HF/UHF (constraints)	H_f[b,c]	$\Delta\Delta H_f$[d]	X_{am}	α_C[e]	α_N[e]
MNic[c]	HF (none)	−452.110 677 5 (0.0)[c]		159.6	2.8	1.8
	UHF (none)	−452.110 677 5 (131.4)		159.6	2.8	1.8
MNic$^{+\cdot}$	UHF (none)	−451.901 299 7		153.3	1.6	0.3
MNic(bent)	HF (bent)	−452.106 416 9	2.7	160.8	17.2	10.9
	UHF (bent)	−452.106 416 9 (133.4)		160.8	17.2	10.9
MNic$^{+\cdot}$ (bent)	UHF (bent)	−451.894 165 3	4.5	154.7	17.0	11.3

[a] See text and Scheme II for structure definitions. [b] Heat of formation in atomic units (hartrees), not corrected for ZPE. [c] Energy differences in parentheses are in kcal/mol (hartrees × 627.51). [d] Difference between planar and boat conformations of MNic and MNic$^{+\cdot}$. [e] Defined in Chart I.

Scheme III

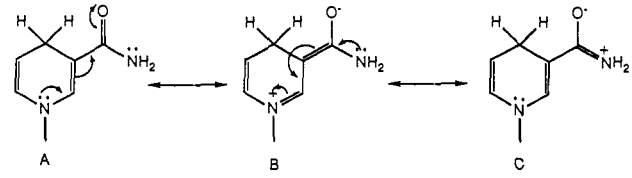

Chart IV

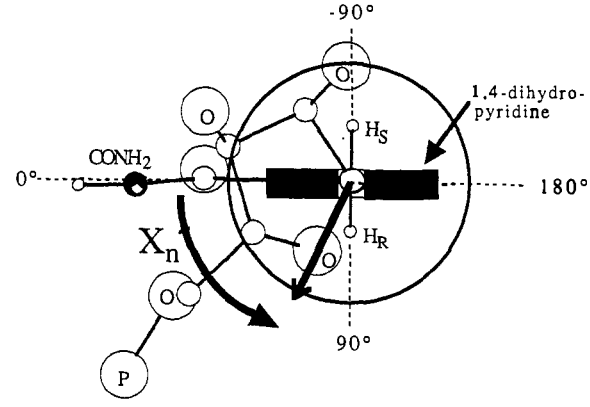

state (2.7 kcal/mol at 3-21G* geometry, UHF singlet). Thus, quasi-boat formation destabilizes the radical cation by about 2 kcal/mol, so that such a conformational change cannot assist the 1e$^-$ oxidation of 1,4-dihydronicotinamide. The puckering angles α_C and α_N for optimized structures indicate that the pyridine rings of MNic and MNic$^{+\cdot}$ are essentially planar, but deviation from planarity is slightly more pronounced for MNic than for MNic$^{+\cdot}$. The value of X_{am} is invariably between 153 and 161° for all structures in Table II. The C=O of the amide remains adjacent to H_S, as is the case in the X-ray structure for catalase and during MD simulation. An interesting observation is that the 3-21G* optimized structures display a tendency toward sp^3-hybridization at NH_2 of the amide. The small but detectable pyramidalization on the nitrogen is associated with a 117° angle for H–N–H of both flat optimized rings and boat forms of MNic and MNic$^{+\cdot}$, which corresponds to a hybridization of $sp^{2.1}$.[19] This could arise from a contribution of the dipolar resonance form B in Scheme III.

The relationship between the ribose and 1,4-dihydronicotinamide rings of the nicotinamide nucleotide is defined by X_n (Chart I). A *syn* conformation is observed, as shown in Chart IV. Figure 8b shows the variation of X_n during MD. X_n is observed to be stable in the dynamics simulation, and the range of values (73–

(19) Calculated from the relation $\cos\varphi = s/(s-1) = (p-1)/p$, where φ is the H–N–H angle and s and p are the percentages of s- and p-character, respectively. See: Huheey, J. E. *Inorganic Chemistry*, 3rd ed.; Harper & Row: New York, 1983; p 227.

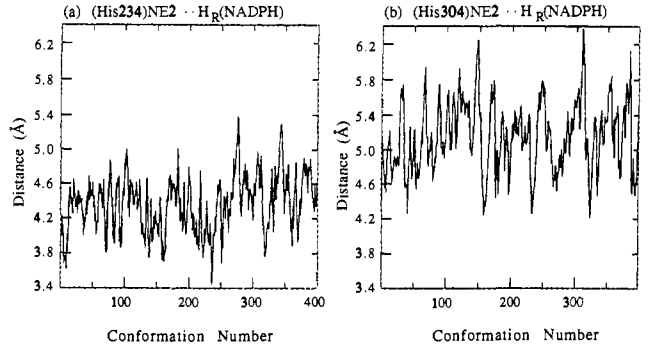

Figure 9. Calculated interatomic distance in catalase from CHARM$_m$ molecular dynamics, 20-ps sampling phase: (a) NE2(His234) to H$_R$(NADPH); (b) NE2(His304) to H$_R$(NADPH).

Chart V

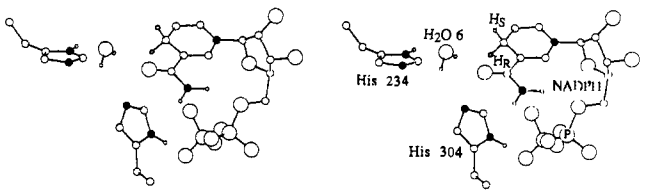

Chart VI

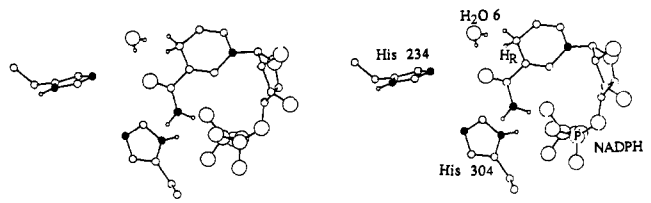

115°) indicates that the endocyclic C–O bond on the ribose assumes a perpendicular arrangement with respect to the nicotinamide ring with an average value of 96°. This is close to the local minimum *syn* conformation determined for β-ribosyl-1,4-dihydronicotinamide by AM1.[11b]

C. General-Base Catalysis. Inspection of the X-ray structure of bovine catalase reveals that there are situated very near C4 of the 1,4-dihydronicotinamide ring (Chart V) two imidazole functional groups of His234 and His304. With hydrogens added to the C4 carbon of NADP, it is estimated that the distances from the C4-H$_R$ of NADPH to the basic ε-nitrogens of the imidazoles (NE2) (assuming neutral imidazoles in the more stable δ-protonated tautomeric form) of His234 and His304 are 4.4 and 5.2 Å, respectively. The His234 and His304 imidazole nitrogens and the C4-H$_S$ are separated by 4.8 and 6.1 Å, respectively. These observations, summarized in Chart VI, raise the question as to the identity of the general base and which hydrogen on the prochiral carbon is removed from the incipient radical cation of NADPH, formed by 1e$^-$ oxidation. Monitoring of the above distances during dynamic simulation reveals that His234 is more likely to be the general base than His304. Also, H$_R$ is more likely to be removed than is H$_S$, due to a shorter distance between H$_R$ and NE2 of His234 (averaging 4.4 Å, Figure 9a) and a desirable angle relationship between C4, H$_R$, and NE2 (C4–H$_R$–N angle averages 125° in MD). The other combinations of histidines and C4-hydrogens were found to have less favorable attack angles and longer distances.

Electron-Transfer-Pathway Calculations. A peptide loop separates the NADPH and iron protoporphyrin-IX cofactors (Chart III), providing a barrier for approach of one to the other. The four subunits of the bovine enzyme are each identical with an NADPH binding site and an iron protoporphyrin-IX. Transfer of an electron from NADPH bound to one subunit of the tetrameric protein to a hypervalent porphyrin in another subunit

Table III. Calculated Tunneling Matrix Elements ε[a] from PATHWAYS II[b] Calculations

	ε values to targets[d]		
donor[c]	(1) Heme vinyl (CAC-HQ22)	(2) Heme Fe (NC-HL3)	(3) H$_2$O(Fe) (O-HL1)
	X-ray		
14-DHN (C4-H$_S$)	1.09×10^{-5} (13.21 Å) path A[e]	1.82×10^{-6} (17.87 Å) path B[e,f]	6.56×10^{-7} (18.40 Å)[h] path B[e,g]
adenine (C2-H)	1.28×10^{-6} (13.30 Å)[i]	1.66×10^{-7} (17.40 Å)[j]	
	Dynamics		
14-DHN (C4-H$_S$)	1.22×10^{-5} (14.58 Å) path B	2.63×10^{-6} (19.09 Å) path B	9.48×10^{-7} (19.56 Å)[g] path B[e]
adenine (C2-H)	1.05×10^{-6} (14.25 Å)[j]	2.26×10^{-7} (18.98 Å)[j]	

[a] See eq 4. [b] See ref 9. [c] Start orbitals: for 14-DHN = C4–HQ2; for adenine = C45–HQ35 (See supplementary material for numbering scheme). [d] Goal orbitals were chosen as follows: (1) for compound I reduction, vinyl terminal on pyrrole ring C of protoporphyrin-IX; (2) for compound II reduction, NC–Fe ligand bond in the plane of the porphyrin; (3) for transfer via axially ligated water molecule on the iron center, O–HL1 lone-pair on the water molecule. The number in parentheses denotes the edge–edge distance from donor to acceptor. [e] For description of paths A and B, see text and charts. [f] Pathway A competes effectively with an ε of 1.41×10^{-6}. [g] Pathway A competes effectively with an ε of 5.09×10^{-7}. [h] Pathway goes through porphyrin ring (essentially pathway B). [i] Phe197–Thr149–Asn148–Asn147–Porphyrin. [j] Much like pathway B.

can be discounted on inspection of the fully assembled tetramer. The subunits bind NADPH such that the porphyrin moiety closest to the dinucleotide is that within the same subunit. On these premises, we used the X-ray structure of a single subunit of bovine catalase as provided in the Brookhaven database[5,14] as coordinates for the PATHWAYS II program.[9] (The latter has been specifically designed to predict pathways for electron tunneling in proteins and small molecules).[17a-c] In addition, structures were extracted from the CHARM$_m$ molecular dynamics simulation, which displayed varying distances between C4-H$_S$ on NADPH and the terminal vinyl H$_2$C=CH- on ring C of the heme (Figure 6b). These coordinates were also used in PATHWAYS II calculations for comparison with the X-ray structure.

Pathways to the Porphyrin Ring: Reduction of Compound I. Table III summarizes coupling factors and pertinent distances calculated using the target orbital CAC-HQ22 of the vinyl terminus of protoporphyrin-IX closest to NADPH. Calculations with the vinyl group orbital as the target can be taken to reflect the efficiency by which the porphyrin cation radical moiety of compound I can be reduced by NADPH in a single-electron transfer. If the electron is expelled from the C4-H$_S$ orbital of the 1,4-dihydronicotinamide ring, Pro150 would be the initial 1e$^-$ mediating residue, since it is the closest residue to C4 in the X-ray structure and during molecular dynamics. The adenine ring of NADPH also comes into contact with Pro150 but can be eliminated from involvement in 1e$^-$ transfer (Table III) on the basis that the nicotinamide ring couples approximately 10 times more strongly with the porphyrin than does the adenine. This is due mainly to the distance that the electron must jump from NADPH to Pro150 and from adenine to Pro150.

Continuing from Pro150, two major contributing pathways to the heme can be identified via PATHWAYS II calculations (Chart VII). Path A (Chart VIII) involves C4-H$_S$–jump–Pro150(3.06 Å)–Thr149–OH–jump–β-carbon on the sidechain of Asn147(2.94 Å)–CH$_2$=PP-IX. The amide sidechain of Asn147 sits between pyrrole ring C and the vinyl group on one side of the heme. Electron transfer from the Cβ-CONH$_2$ of Asn147 to the protoporphyrin-IX vinyl group is facilitated because these entities are in van der Waals contact (X-ray structure). Path B (Chart IX) is favored in a snapshot structure from

Chart VII

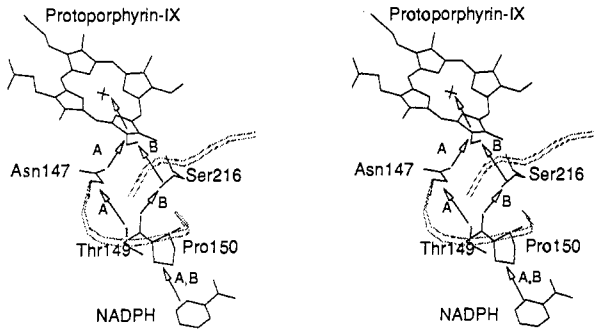

Chart VIII

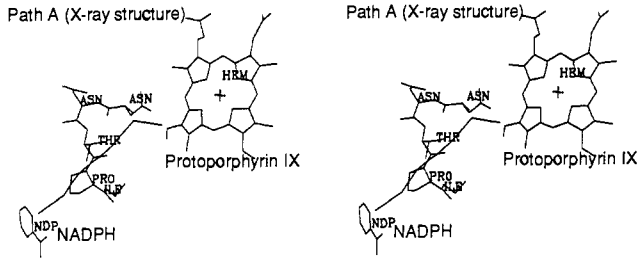

Chart IX

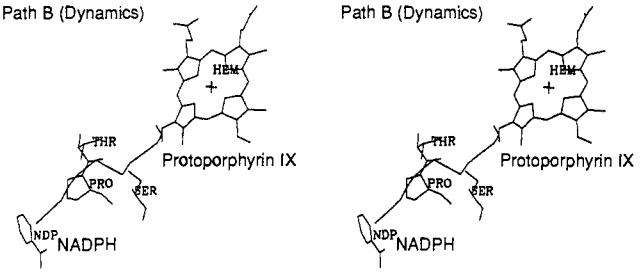

dynamics simulation and consists of Pro150–Thr149(C=O)–Hbond–Ser216–CH_2OH–jump–(3.31 Å)CH_2=PP-IX. The motion of the enzyme structure in MD brings the -OH of Ser216 into position to form a tight interstrand hydrogen bond with the carbonyl oxygen of Thr149. Ser216 is also in close contact with pyrrole ring C of the heme, and a through-space jump is facilitated. The calculated coupling efficiencies (ϵ-values) of pathways A and B are within a factor of 10 of one another, and these two paths are preferred 10–100-fold over other possible pathways. The chosen dynamics structure provides the most favorable pathway (Path B). This is related to the fact that the dynamics structure has the shortest jump between C4-H_S and Pro150 (2.90 Å). The edge to edge distance is greater for the dynamics structure (14.6 vs 13.2 Å), but this is not as important as the size of the initial jump.

Pathways to the Iron Center: Reduction of Compound II. Reduction of compound II (iron(IV) oxo porphyrin) is metal centered, and therefore, one must complete the pathway by calculating couplings using the ligand–iron orbitals as targets. The choice of the NC–HL3 ligand orbital as the target for metal-center reduction was made since NC is the pyrrole nitrogen closest to NADPH. As seen in Table III, ϵ values are calculated to be approximately 5-times smaller than calculated when the vinyl terminal is the target. It was found that the best pathways to the iron center invariably involved path B to the edge of the porphyrin with completion of the pathway through the skeleton of the ring. An interesting question arises as to the possibility of employing the catalytic His74[20] to transfer the electron to iron via an H_2O (or H_2O_2 or =O) ligand. Path A could be traversed to Asn147, which contacts the catalytic His74. This possibility is not available

(20) Fita, I.; Rossmann, M. G. *J. Mol. Biol.* **1985**, *185*, 21.

Scheme IV

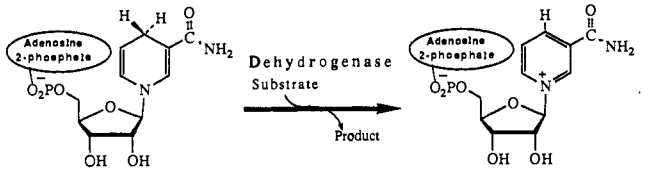

in the selected dynamic structure because the sidechain of Asn147 has moved away from both the PP-IX and His74. With H_2O as ligand, in both the X-ray and dynamics structure, the electron tunneling to the iron hydrate was judged using PATHWAYS II. The results (Table III) indicate that the best paths to the water ligand on iron go through the porphyrin ring. In separate calculations with the His74 ND–HQ5 orbital as the initial target, it was found that transfer via His74 to Fe–OH_2 is considerably less efficient (by >100-fold) than the A and B pathways already identified.

It is interesting to note that all the plausible electron-tunneling pathways are on the catalytic distal side of the porphyrin such that the proximal ligand Tyr357 plays no significant role. Hydrogen peroxide likely approaches the distal side by passing between Asn147 and Val115,[20] very close to the predicted major pathway for electron transfer (Chart VIII). Finally, it should be noted that choices of electron-tunneling pathways predicted by use of PATHWAYS II calculations are very sensitive to the values chosen for the standard driving force (in this study β = 1.7 $Å^{-1}$) and the prefactor term in the general distance-dependent coupling relationship of eq 4. Decreasing the value of the prefactor in the hydrogen-bond term ϵ^{HB} from 0.6 to 0.3 results in approximately equal magnitudes of coupling for pathways A and B by underestimating the hydrogen bond between Ser216 and Thr149.

Discussion

Enzymatic and nonenzymatic reductions by dihydropyridines involve hydride (concerted two-electron–proton) transfer (Scheme IV).[21] Single-electron reductions by 1,4-dihydropyridines are observed when the oxidant has a positive reduction potential and can provide a stable radical or is an obligate one-electron oxidant (eq 5).[13,22] The function of enzyme-bound NADPH to reduce compound II of catalase was first considered by Kirkman and co-workers.[23] Jouve et al. found that the presence of NADPH led to a decrease in compound II formation in *P. mirabilis* catalase, supporting the former suggestion.[6] Approximately 20 Å separate the iron center and the 1,4-dihydronicotinamide ring, and there are some 13.7 Å separating the 1,4-dihydronicotinamide and the closest terminal vinyl group on pyrrole ring C of protoporphyrin-IX.[5] An extended peptide sequence physically separates the 1,4-dihydronicotinamide and porphyrin. Direct hydride transfer between NADPH and compounds I and II can be dismissed. Hydrogen tunneling is judged impossible over the distance required. Bound NADPH must serve as a one-electron donor to reduce compound II to the resting-state iron(III) protoporphyrin-IX (eq 12). Presumably, general-base catalysis of proton removal

$$\begin{array}{c}\text{catalase–(porph)}Fe^{IV}O \\ + \\ \text{NADPH}\end{array} \rightarrow \begin{array}{c}\text{catalase–(porph)}Fe^{III} \\ + \\ \text{NADPH}^{+\bullet}\end{array} \qquad (12)$$

and $1e^-$ transfer to an oxygen or other small molecule would complete the reaction (eq 13). The question whether NADPH bound to catalase can react with compound I has been largely left

(21) (a) Mauzerall, D.; Westheimer, F. H. *J. Am. Chem. Soc.* **1955**, *77*, 2261. (b) Abels, R. H.; Hutton, R. F.; Westheimer, F. H. *J. Am. Chem. Soc.* **1957**, *79*, 712.

(22) Powell, M. F.; Bruice, T. C. In *Oxidases and Related Redox Systems*; Alan R. Liss, Inc.: New York, 1988; pp 369–385.

(23) Kirkman, H. N.; Galiano, S.; Gaetani, G. F. *J. Biol. Chem.* **1987**, *262*, 660.

$$NADPH^{+\bullet} + B: \rightarrow NADP^{\bullet} + BH^{+} \xrightarrow{O_2} NADP^{+} + O_2^{-\bullet} \quad (13)$$

unanswered. However, if catalase should encounter a very dilute solution of H_2O_2 such that the compound I species would be long-lived before a turnover with a second H_2O_2, then the protoporphyrin-IX ring structure and/or the protein could be oxidized. A comparison of the potentials for $1e^-$ reduction of compounds I and II in horseradish peroxidase C (0.96 and 0.94 V vs SHE, respectively)[24] shows them to be comparable, such that the reactions of eqs 14, 15, and 16 should be important. A

$$\begin{array}{c} \text{catalase–(porph}^{+\bullet}\text{)Fe}^{IV}\text{O} \\ + \\ \text{NADPH} \end{array} \rightarrow \begin{array}{c} \text{catalase–(porph)Fe}^{IV}\text{O} \\ + \\ \text{NADPH}^{+\bullet} \end{array} \quad (14)$$

$$NADPH^{+\bullet} + B: \rightarrow NADP^{\bullet} + BH^{+} \quad (15)$$

$$\begin{array}{c} \text{catalase–(porph)Fe}^{IV}\text{O} \\ + \\ \text{NADP}^{\bullet} \end{array} \rightarrow \begin{array}{c} \text{catalase–(porph)Fe}^{III} \\ + \\ \text{NADP}^{+} \end{array} \quad (16)$$

difficulty in investigating this feature is the problem of preparation of compound I in the absence of any peroxide. Hillar and Nicholls have recently suggested that compound I can form a new species by capturing an electron from an amino acid sidechain. By transferring a single oxidation equivalent from the porphyrin to a residue in the protein, the system retains the two oxidation equivalents and the NADPH can supply both reducing equivalents to quench them.[25] If one of the oxidation equivalents is lost, however, the second electron from $NADPH^{+\bullet}$ is expected to dissipate by reaction with an exogenous oxidant, such as O_2. It has been found previously that $NADP^{\bullet}$ reacts rapidly with dioxygen to give $O_2^{-\bullet}$.[26] Although compound II in catalase is inactive in the catalytic cycle of the enzyme, iron(IV) oxo tetraphenylporphyrin models for compound II react with hydrogen peroxide to give superoxide.[27]

While there are chemical examples of one-electron transfer from 1,4-dihydropyridines to obligate one-electron acceptors,[13] the quenching of compounds I and II are rare biochemical examples of NAD(P)H acting as a $1e^-$ reductant. The reduction of ferrocenium cations by *N*-benzyl-1,4-dihydronicotinamide[28] or NADH[29] involves electron–proton–electron transfer with the first $1e^-$ transfer being rate limiting. The reactions are characterized by a lack of sensitivity to pH and buffer concentration and show no deuterium isotope effect. Scheme I has been established in this study to represent the $1e^-$, H^+, $1e^-$ oxidation of a 1,4-dihydropyridine with $Fe(CN)_6^{3-}$ (Scheme I). Ferricyanide has a reduction potential of 460 mV,[30] approaching the range of the potentials for metal porphyrin compound I in peroxidases.[24] When the first $1e^-$ transfer is not rate determining, general-base catalysis of the deprotonation of $MAH^{+\bullet}$ can be established. The relatively large deuterium isotope effects (k_2^H/k_2^D = 5–10 by use of MAH and MAD) support a rate-determining deprotonation of $MAH(D)^{+\bullet}$ to give the neutral radical $MA^{\bullet}$. Finally, a Brønsted coefficient of $\beta = 0.2$ indicates an early transition state for general-base-catalyzed deprotonation of $MAH^{+\bullet}$. An early transtion state associated with a large kinetic deuterium isotope effect is suggestive of proton tunneling.[31]

Consider the mechanism of Scheme V to represent the role of NADPH in the quenching of compound I of catalase. In Scheme V the initial electron transfer may well be rate limiting, since the electron must travel through the peptide backbone and, to a limited extent, through space. The peptide segment which separates the porphyrin and NADPH probably serves to attenuate the electron-transfer rate to such an extent that compound I possesses a lifetime sufficient for turnover with H_2O_2. Second, an imidazole from His234 is situated in a favorable juxtaposition so as to function as a general base to remove a proton from C4 of $NADPH^{+\bullet}$ (Figure 9a). The enforced proximity of the base and H_R could result in a large rate enhancement of the deprotonation step in the catalase reaction when compared to the intermolecular reactions of Scheme I. It is known that the pK_a for dissociation of the C10–H bond of MAH is decreased to the pK_a range of imidazole upon oxidation to $MAH^{+\bullet}$.[32] Though inspection of the X-ray structure of catalase (Chart V) indicates that His304 should play the role of general-base catalyst, MD simulations show His234 as the more likely candidate (Chart VI).

On the basis of PATHWAYS II[9] calculations, electron transfer from NADPH to iron protoporphyrin-IX (PP-IX) may occur by two major pathways. Path A is the preferred path from the X-ray structure, and path B is the favored path from a pic structure obtained on molecular dynamics. These pathways are as follows: A (Chart VIII), 14DHN(C4-H_S)–jump–Pro150–Thr149–jump–Asn147–CH_2CONH_2–jump–vinyl H_2C=(PP-IX); and B (Chart IX), 14DHN(C4–H_S)–jump–Pro150–Thr149(C=O)–Hbond–(H–O)Ser216–jump–vinyl H_2C=(PP-IX). The NH_2 of the amide sidechain of Asn147 has been implicated in the catalysis of decomposition of hydrogen peroxide ligated to the iron porphyrin.[20] This raises the possibility of a dual role of this sidechain in enzyme catalysis and electron transfer. Assuming compound I (iron(IV) oxo porphyrin π-cation radical) as target, the most facile means for the first electron transfer is to the porphyrin π-cation-radical ring via Asn147. For the reduction of compound II, an electron must be delivered to iron(IV). Computations suggest that all transfers of electrons from NADPH, whether to compound I or compound II, go directly from the nicotinamide ring through the protein to the edge of the porphyrin ring. Both paths A and B are rather direct such that they satisfy the least distance–best path rule of Dutton[33] and the concept of a broad path of shortest distances as proposed by Kuki.[34]

Molecular dynamics calculations with the X-ray structure of catalase establish that the 1,4-dihydropyridine ring of NADPH preferentially assumes a quasi-boat conformation by bending away from the adenosine ribose ring. Ab initio calculations at the 3-21G* level in the Gaussian 90 program revealed differences in oxidation potential for planar and quasi-boat conformations of *N*-methyl-1,4-dihydronicotinamide [MNic and MNic(bent)] which indicate that no kinetic advantage can be derived from anisotropic puckering of the 1,4-dihydropyridine ring. The anisotropy of the quasi-boat formation in dynamics (Figure 7) shows that the pseudo-axial H_S is pointed toward the peptide loop, separating the NADPH and protoporphyrin-IX. Perhaps this enforces proximity of H_S to Pro150 and facilitates $1e^-$ transfer. It is interesting to note that in dehydrogenases, the anisotropic

(24) Hayashi, Y.; Yamazaki, I. *J. Biol. Chem.* **1979**, *254*, 9101.
(25) Hillar, A.; Nicholls, P. *FEBS Lett.* **1992**, *314*, 179.
(26) (a) De Sandro, V.; Dupuy, C.; Kaniewski, J.; Ohayon, H.; Deme, D.; Virion, A.; Pommier, J. *Eur. J. Biochem.* **1991**, *201*, 507. (b) Yokota, K.; Yamazaki, I. *Biochemistry* **1977**, *16*, 1913. (c) Land, E. J.; Swallow, A. J. *Biochim. Biophys. Acta* **1971**, *234*, 34.
(27) (a) Lindsay Smith, J. R.; Balasubramanian, P. N.; Bruice, T. C. *J. Am. Chem. Soc.* **1988**, *110*, 7411. (b) Balasubramanian, P. N.; Lindsay Smith, J. R.; Davies, M. J.; Kaaret, T. W.; Bruice, T. C. *J. Am. Chem. Soc.* **1989**, *111*, 1477.
(28) Miller, L. L.; Valentine, J. R. *J. Am Chem. Soc.* **1988**, *110*, 3982.
(29) Carlson, B. W.; Miller, L. L.; Neta, P.; Grodkowski, J. *J. Am Chem. Soc.* **1984**, *106*, 7233.
(30) Clark, W. M. *Oxidation-Reduction Potentials of Organic Systems*; R. E. Kreiger: Huntington, NY, 1972; p 132.
(31) (a) Melander, L. *Isotope Effects on Reaction Rates*; Ronald Press: New York, 1960; pp 24–32. (b) Westheimer, F. H. *Chem. Rev.* **1961**, *61*, 265.
(32) The pK_a values for MAH and MAD in wet acetonitrile have been directly determined: Fukuzumi, S.; Tokuda, Y. *Chem. Lett.* **1992**, 1721.
(33) Dutton, P. L. *Nature* **1992**, *355* (6363), 796.
(34) Kuki, A. Private communication.

Scheme V

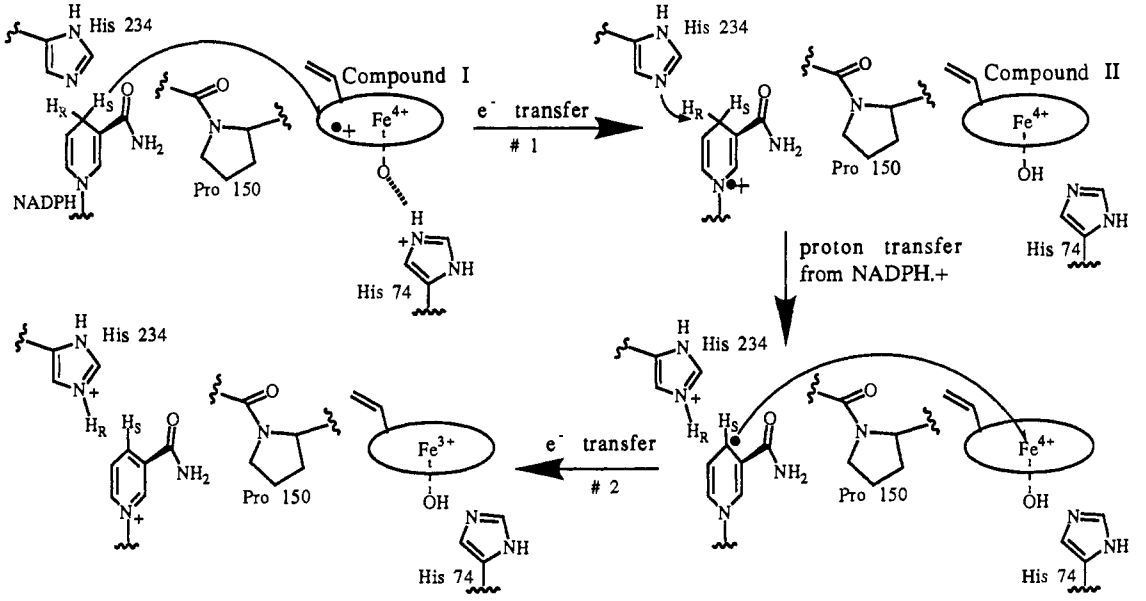

quasi-boat conformation is predicted to have significant kinetic advantage over planar conformations.[11b] A persistent *trans* conformation for the amide (Chart II and Figure 8a) is observed in NADPH bound to catalase during dynamics simulation. The *trans* conformation is held by hydrogen bonding with the pyrophosphate linkage, while in dehydrogenase structures, the *trans* conformation is enforced by the amide being associated with hydrogen-bond acceptors on the protein. A major difference between the binding domain for NADPH in catalase and the binding sites in NAD(P)H dehydrogenases is that NADPH in catalase is folded such that 1,4-dihydronicotinamide and adenine rings approach one another.[5] Observed X_{am} values (Figure 8a) indicated that the C=O remains on the B-face of the 1,4-dihydronicotinamide ring. The anisotropy of the amide conformation contrasts the behavior seen in lactate dehydrogenase under similar conditions[11b] and could suggest a functional role for the amide in the mechanism for NADPH oxidation in catalase. The carboxamide sidechain of 1,4-dihydronicotinamide has been suggested to impart a catalytic effect on the rate of hydride reductions by NAD(P)H dehydrogenases.[35] The carbonyl oxygen of the amide can possibly add directionality to electron transfer from NADPH by fixing its orientation toward the electron acceptor. Finally, the small, but observable pyramidalization of the amide NH_2 in the 3-21G* calculated optimum structures toward $sp^{2.1}$ implies that dipolar forms such as B in Scheme III can contribute to the overall electronic structure of MNic.[36] In the oxidized nicotinamide, this resonance structure is not possible, and a rehybridization of NH_2 to $sp^{2.0}$ is probable.

In conclusion, we have constructed a plausible mechanism of one-electron oxidation of NADPH with general-base catalysis in catalase, based on kinetic studies, structural data, molecular dynamics simulation, and calculations of electron-tunneling pathways. When compound I is quenched (Scheme V), both reducing equivalents of NADPH are used, while compound II requires only one. Therefore, the second electron will dissipate by reaction with an exogenous oxidant, such as O_2. It is suggested that NADPH in catalase plays the role of a fuse, which will go off in instances where (a) compound II accumulates at the active site or (b) the highly unstable compound I (or a compound II–protein radical couple, as suggested by Hillar and Nicholls[25]) is allowed to sit in the absence of substrate. Thus, NADPH is a rescuer of inactive catalase and a device to defuse compound I to prevent oxidative damage to heme or protein.

Acknowledgment. This study was supported by grants from the National Science Foundation and the Office of Naval Research. Ö.A. expresses appreciation to the Jón Pórarinsson Educational Fund for a fellowship. Gratitude is extended to Jeffrey J. Regan for supplying PATHWAYS II and for valuable discussions.

Supplementary Material Available: A Gaussian *Z*-matrix for the optimized structure of $MNic^{+\bullet}$ and a potential specification file for use in PATHWAYS II with parameters for NADPH and a numbering scheme for the cofactor (4 pages). Ordering information is available on any current masthead page.

(35) (a) Donkersloot, M. C. A.; Buck, H. M. *J. Am. Chem. Soc.* **1981**, *103*, 6554. (b) Beijer, N. A.; Buck, H. M.; Sluyterman, L. A. A.; Meijer, E. M. *Biochim. Biophys. Acta* **1990**, *1039*, 227.

(36) Rotberg and Cleland have suggested the participation of a dipolar resonance structure **B** in Scheme III in NADH bound to dehydrogenases: Rotberg, N.; Cleland, W. W. *Biochemistry* **1991**, *30*, 4068.